AIP | Applied Physics Letters

An underlap field-effect transistor for electrical detection of influenza

Kwang-Won Lee, Sung-Jin Choi, Jae-Hyuk Ahn, Dong-Il Moon, Tae Jung Park et al.

Citation: Appl. Phys. Lett. **96**, 033703 (2010); doi: 10.1063/1.3291617
View online: http://dx.doi.org/10.1063/1.3291617
View Table of Contents: http://apl.aip.org/resource/1/APPLAB/v96/i3
Published by the American Institute of Physics.

Additional information on Appl. Phys. Lett.

Journal Homepage: http://apl.aip.org/
Journal Information: http://apl.aip.org/about/about_the_journal
Top downloads: http://apl.aip.org/features/most_downloaded
Information for Authors: http://apl.aip.org/authors

ADVERTISEMENT

Downloaded 31 May 2013 to 210.123.42.187. This article is copyrighted as indicated in the abstract. Reuse of AIP content is subject to the terms at: http://apl.aip.org/about/rights_and_permissions

An underlap field-effect transistor for electrical detection of influenza

Kwang-Won Lee,[1] Sung-Jin Choi,[1] Jae-Hyuk Ahn,[1] Dong-Il Moon,[1] Tae Jung Park,[2] Sang Yup Lee,[2,3] and Yang-Kyu Choi[1,a)]

[1]*School of Electrical Engineering and Computer Science, Division of Electrical Engineering, KAIST, Daejeon 305-701, Republic of Korea*

[2]*BioProcess Engineering Research Center, Center for Systems and Synthetic Biotechnology, and Institute for the BioCentury, KAIST, Daejeon 305-701, Republic of Korea*

[3]*Department of Bio and Brain Engineering, Department of Biological Sciences, and Bioinformatics Research Center, KAIST, Daejeon 305-701, Republic of Korea*

(Received 29 September 2009; accepted 18 December 2009; published online 21 January 2010)

An underlap channel-embedded field-effect transistor (FET) is proposed for label-free biomolecule detection. Specifically, silica binding protein fused with avian influenza (AI) surface antigen and avian influenza antibody (anti-AI) were designed as a receptor molecule and a target material, respectively. The drain current was significantly decreased after the binding of negatively charged anti-AI on the underlap channel. A set of control experiments supports that only the biomolecules on the underlap channel effectively modulate the drain current. With the merits of a simple fabrication process, complementary metal-oxide-semiconductor compatibility, and enhanced sensitivity, the underlap FET could be a promising candidate for a chip-based biosensor. © *2010 American Institute of Physics*. [doi:10.1063/1.3291617]

A variety of biosensors, such as, optoelectronic devices,[1] magnetostrictive microcantilever,[2] conductometric devices,[3] and field-effect transistor (FET) type sensors[4,5] have been recently reported to create functional biosensor systems. Among several types of concepts, a FET-based sensor has attracted public attention owing to its various advantages related to miniaturization, standardization, and mass-production. As one of the most promising FET-type devices, an ion-selective FET (Ref. 6) utilizing a reference electrode in an aqueous solution and nanowire FETs[7,8] employing a one-dimensional nanowire to exhibit conductance change as a sensing parameter have a sufficiently high sensitivity to detect a small amount of biomolecules. However, these FET-type biosensors lack compatibility with the standard complementary metal-oxide-semiconductor (CMOS) process and monolithic integration for the construction of readout circuits and signal processing systems. Moreover, a nanogap-embedded device named as a dielectric-modulated FET (DMFET) was recently demonstrated as another type of biosensor.[9] It's electrical detection method involves monitoring the change of the threshold voltage which originates from the change of the gate dielectric constant as a result of immobilized biomolecules in the nanogap. Due to the partial modification of a conventional metal-oxide-semiconductor FET (MOSFET), DMFET has the merits of high compatibility with the CMOS process and adaptability to readout circuits compared to previous FET-type biosensors. However, it is also associated with the limitations of low binding probability in a carved nanogap and a low structural stability stemming from the mechanically suspended nanogap structure.

In this letter, a revamped FET-type biosensor that encloses the underlap structure is proposed to solve the aforementioned problems with preceding FET-type biosensors. Through the structural modification of a conventional MOSFET, the underlap device has all the advantages of the DMFET as well as additional merits due to the characteristics of the underlap structure. Due to the prominent open structure, unlike a concave-carved nanogap, biomolecules have additional opportunities to bind to a designed area. The simplicity of the fabrication process and the degree of structural stability are additional advantages of the underlap device. Additionally, more of a current change can be observed compared to a nanogap FET device, as the channel potential in the underlap region is very sensitive to external charges. Thus, by detecting changes in the drain current, targeted molecules can be electrically detected without a labeling process of biomolecule.

Figure 1(a) shows a schematic of the drain side underlap device fabricated with an intentional offset between the gate and the channel region. Local oxidation of silicon was formed on a p-type silicon wafer to suppress the device-to-device leakage current. The source/drain (S/D) was made by arsenic ion-implantation and activated by subsequent thermal annealing. Silicon oxide (SiO_2) at a thickness of 20 nm was

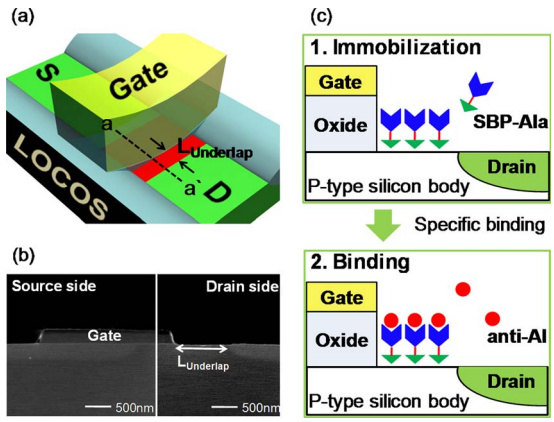

FIG. 1. (Color online) (a) Schematic of the fabricated underlap FET device, (b) S/D profile image by SEM of the underlap-embedded FET, and (c) cross-sectional image of the underlap region and schematic representation of the SBP-AIa and anti-AI binding in the underlap region.

a)Electronic mail: ykchoi@ee.kaist.ac.kr.

 © 2010 American Institute of Physics

Downloaded 31 May 2013 to 210.123.42.187. This article is copyrighted as indicated in the abstract. Reuse of AIP content is subject to the terms at: http://apl.aip.org/about/rights_and_permissions

thermally grown as a gate dielectric layer. The n-type *in situ* doped polycrystalline layer was sequentially deposited and patterned. The underlap region between the edge of the gate and the S/D at various lengths was intentionally designed to include an offset. The scanning electron microscopic (SEM) image taken at a low energy of 1 keV clearly shows that the drain region is apart from the gate edge as shown in Fig. 1(b). Thereby, the uncovered channel region assigned for the sensing area is adequately constructed.

To investigate validity of the underlap device as a biosensor, silica-binding proteins (SBP), which strongly bind to the oxide surface at one end and combine with the avian influenza surface antigen (AIa), the biomolecule receptor, at the other end, were designed by recombinant technology.[10] Therefore, the AIa was effectively immobilized onto the oxide surface without an additional surface modification. Moreover, SBP-fusion protein could control the receptor orientation resulting on regular distance between the analyte and the sensing surface. Figure 1(c) shows a cross-sectional schematic strategy (a-a′) of SBP fused with the AI antigen (SBP-AIa) anchored onto the underlap region and anti-AI antibody (anti-AI), which was purified from polyclonal antibody immunized in a rabbit by Peptron (Korea),[10] bound with SBP-AIa. It is well known that native oxide was grown on the underlap region and on other crystalline or polycrystalline silicon surfaces whenever these substances are exposed to air ambient. In order to combine anti-AI with the oxide surface, the underlap device was immersed in the SBP-AIa solution diluted in phosphate-buffered saline (PBS) (pH 7.4) solution for 1 h. Subsequently, the device was thoroughly rinsed with de-ionized water (DW) and dried with N_2-gas. Thereafter, the same process to immobilize the anti-AI is carried out to the SBP-AIa-immobilized underlap device.

The fabricated underlap device has a channel length of 10 μm, a channel width of 20 μm, and various underlap lengths from 100 to 1400 nm. Figure 2(a) shows the drain current versus the gate voltage characteristics as a parameter of the underlap length. A device with a longer underlap length shows more of a threshold voltage (V_T) shift in the positive direction, and the overall V_T shift is approximately 1.2 V compared to a normal overlap device. A higher gate voltage is required due to the fact that it is more difficult to invert the underlap channel without the gate directly straddling the channel. Figure 2(b) demonstrates the change of V_T after varying the underlap length for both the drain and source side. A method to switch the electrical direction of the underlap in an exchange of the source and drain electrode was used. At the source side underlap, V_T increases in all bias conditions when V_{DS}=0.05 and 1 V, respectively. In contrast, V_T increases only when V_{DS}=0.05 V at the drain side underlap. That is, in the condition of a high drain bias, the V_T value of the drain side underlap device is nearly identical to that of the overlap device. The channel potential at the underlap region is lowered significantly by a reduction in the potential barrier width which is caused by the high drain bias. Subsequently, the V_T change is negligible at a high drain bias. On the other hand, at the source side underlap, the drain bias effects do not have an impact on the channel potential because the potential barrier width is formed at the source underlap region regardless of the high drain bias. This is an important property of the underlap device.

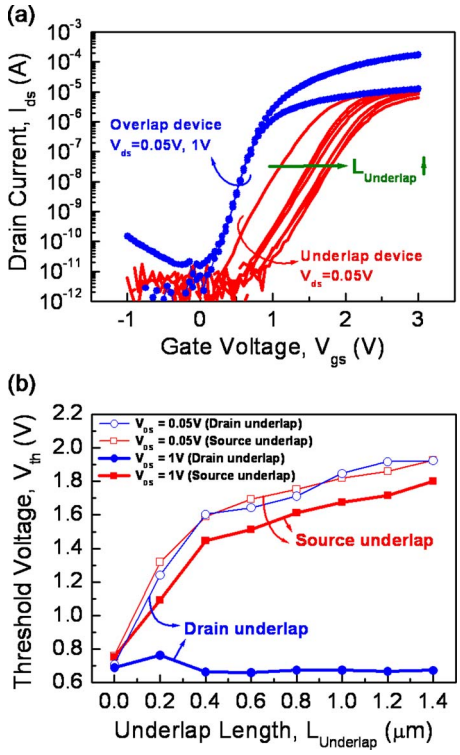

FIG. 2. (Color online) (a) The transfer characteristics of the overlap device at drain biases of 0.05 and 1 V and an underlap device for various underlap lengths at 0.05 V, (b) extracted V_T values of both the underlap and overlap device as a function of the underlap length at drain biases of 0.05 and 1 V. V_T was read at a constant drain current of 100 nA.

To investigate the effectiveness of the underlap device as a biosensor, the bioexperiment was carried out using 25 μg/ml of a SBP-AIa solution and 10 μg/ml of an anti-AI solution. Figure 3(a) shows the transfer characteristics in each bioexperimental state of the 900 nm underlap length device. Figure 3(b) was reconstructed to show how the drain current is effectively changed as a result of the reaction between the SBP-AIa and the anti-AI. V_T also shifted remarkably in consequence. As shown in the inset of Fig. 3(a), after the immobilization of SBP-AIa, the drain current increases slightly in comparison to that in the initial state. The small increment of the drain current can be explained by the presence of an additional fringing field due to the immobilized SBP-AIa, of which the thickness is approximately 3 nm on the underlap region. However, by binding of anti-AI molecules with the SBP-AIa at the underlap region, the drain current decreases considerably in all various underlap devices. The abrupt drop of the drain current is attributed to the negative charges of the anti-AI, and the decrement in the drain current becomes larger as the underlap length increases. The number of inverted electrons in the channel of the underlap region is reduced by the negatively charged anti-AI. In the band diagram, the electron barrier height formed by the underlap structure is elevated by the negative anti-AI charges. This effect is in good agreement with an explanation of the drain current reduction; this was verified with the aid of a numerical simulation.[11] Although anti-AI has only small negative charges, the charge effect on the channel is more dominant than the additional fringing field effect caused by the change of the dielectric constant. Thus, a noticeable drop of the drain current was observed. On the other hand, with a zero underlap length, i.e., a conventional

Downloaded 31 May 2013 to 210.123.42.187. This article is copyrighted as indicated in the abstract. Reuse of AIP content is subject to the terms at: http://apl.aip.org/about/rights_and_permissions

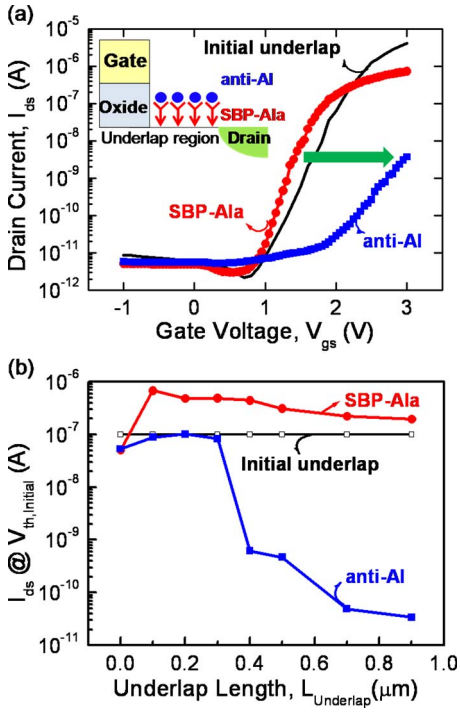

FIG. 3. (Color online) (a) The transfer characteristics in each stage of a bioexperiment in a device with an underlap length of 900 nm; the initial underlap device, the immobilization of SBP-AIa, and the binding of anti-AI are shown. The inset is a schematic showing the biomolecule immobilization process in the underlap region and (b) extracted drain current at its initial V_T after each stage of the bioexperiment for various underlap lengths.

overlap device, there is no change in the current after the binding of the anti-AI. As a result, it was verified that the change in the drain current comes from only the binding of anti-AI at the underlap region.

To prove that the current change is caused by the specific binding of the SBP-AIa and anti-AI elements, a recovery experiment to break the binding sites of the biomolecules was conducted. In order to detach the bound proteins from the surface, an underlap device with SBP-AIa and anti-AI was immersed in the 90 °C DW (Ref. 12) for 10 min and rinsed with DW several times. The drain current was restored back to its initial value due to the separation of the biomolecules as shown in Fig. 4. As another control experiment, the 34-mer single-stranded DNA (ssDNA) known to have negative charges was selected for a control bioexperiment to show that the negative charges of anti-AI bring about a current change. Figure 4 shows the change in the drain current during the process of 3-aminopropyltriethoxysilane as a self-assembled monolayer[13] to attach the ssDNA and after its immobilization. In a comparison to the anti-AI result, the change tendency shows the same characteristics. Consequently, it can be inferred that the change in the drain current is mainly dominated by the negative charges of the underlap region. Moreover, a bioexperiment for a false positive test with the nonspecific binding of antirabbit immunoglobulin (IgG) was carried out. Due to the nonspecific binding between the SBP-AIa and IgG, there was a little decrease of the drain current, as shown in Fig. 4. Also, as another false positive test, the initial underlap device was directly immersed in

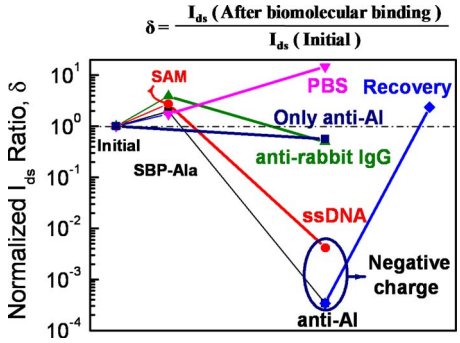

FIG. 4. (Color online) Comparative anti-AI results at an underlap length device of 900 nm; a recovery test to break the specific binding, a ssDNA test to prove the negative charge effect, a false-positive test with nonspecific biomolecules of anti-rabbit IgG, the anti-AI without the SBP-AIa, and the PBS without anti-AI test as a negative control experiment were conducted.

anti-AI solution without the immobilization of the SBP-AIa. As predicted, no significant decrease of the drain current was observed because of the nonspecific binding between anti-AI and SiO_2 surface. These results showed that the underlap-based FET as a biosensor can selectively detect targeted biomolecules. Finally, to examine the effect of the buffer solution, a PBS solution which did not contain anti-AI was selected as a negative control experiment. These results, depicted in the Fig. 4, show that the drain current was slightly increased by the incorporated positive ions in the PBS solution. Accordingly, it proves that the main factor of current decrement is not from PBS but from anti-AI.

In summary, the underlap-embedded FET is shown to detect biomolecules. When SBP-AIa and anti-AI were bound in the underlap channel region, the drain current was significantly modulated by the negative anti-AI charges. From the several control experiments, it was concluded that the change in the drain current resulted only from the biomolecules in the underlap channel region.

This research was supported by the National Research and Development Program (Grant No. 2005-01274) for the development of biomedical function monitoring biosensors and by the NRL program through KOSEF (Grant. No. R0A-2007-000-20028-0).

[1]V. S. Y. Lin, K. Motesharei, K. P. S. Dancil, M. J. Sailor, and M. R. Ghadri, Science **278**, 840 (1997).
[2]S. Li, L. Orona, Z. M. Li, and Z.-Y. Cheng, Appl. Phys. Lett. **88**, 073507 (2006).
[3]M. A. Reed, C. Zhou, C. J. Muller, T. P. Burgin, and J. M. Tour, Science **278**, 252 (1997).
[4]C. Bartic, A. Campitelli, and S. Borghs, Appl. Phys. Lett. **82**, 475 (2003).
[5]G. Shekhawat, S. H. Tark, and V. P. Dravid, Science **311**, 1592 (2006).
[6]P. Bergveld, Sens. Actuators B **88**, 1 (2003).
[7]J. Hahm and C. M. Lieber, Nano Lett. **4**, 51 (2004).
[8]G. F. Zheng, F. Patolsky, Y. Cui, W. U. Wang, and C. M. Lieber, Nat. Biotechnol. **23**, 1294 (2005).
[9]H. Im, X.-J. Huang, B. Gu, and Y.-K. Choi, Nat. Nanotechnol. **2**, 430 (2007).
[10]B. Gu, T. J. Park, J.-H. Ahn, X.-J. Huang, S. Y. Lee, and Y.-K. Choi, Small **5**, 2407 (2009).
[11]Medici User Guide, Version Z-2007.03, March 2007, SYNOPSYS.
[12]A. Holmberg, A. Blomstergren, O. Nord, M. Lukacs, J. Lundeberg, and M. Uhlén, Electrophoresis **26**, 501 (2005).
[13]Y. Cui, Q. Wei, H. Park, and C. M. Lieber, Science **293**, 1289 (2001).

Downloaded 31 May 2013 to 210.123.42.187. This article is copyrighted as indicated in the abstract. Reuse of AIP content is subject to the terms at: http://apl.aip.org/about/rights_and_permissions